CHEMISTRY OF MATERIALS
Cite This: Chem. Mater. 2019, 31, 3624−3635
Article
pubs.acs.org/cm

SF_4 as the Fluorination Reactant for Al_2O_3 and VO_2 Thermal Atomic Layer Etching

Jonas C. Gertsch,[†] Austin M. Cano,[†] Victor M. Bright,[‡] and Steven M. George*,[†]

[†]Department of Chemistry and [‡]Department of Mechanical Engineering, University of Colorado, Boulder, Colorado 80309, United States

ABSTRACT: Thermal atomic layer etching (ALE) is an important technique for the precise isotropic etching of nanostructures. Thermal ALE of many materials can be achieved using a two-step fluorination and ligand-exchange reaction mechanism. Most previous thermal ALE processes have used HF as the fluorination reactant. Alternative fluorination reactants may be needed because HF is a weak nucleophilic fluorination reactant. Stronger fluorination agents may be required for the fluorination of some materials. To demonstrate the usefulness of SF_4 as an alternative to HF, thermal Al_2O_3 ALE was compared using SF_4 or HF together with $Sn(acac)_2$ as the metal precursor for ligand exchange. SF_4 and HF were observed to behave similarly as fluorination reactants during Al_2O_3 ALE. The mass gains during the initial SF_4 and HF exposures on Al_2O_3 atomic layer deposition (ALD) films at 200 °C were comparable at 35 and 38 ng/cm^2, respectively, using quartz crystal microbalance measurements. In addition, the etch rates were similar at 0.20 and 0.28 Å/cycle for Al_2O_3 ALE using SF_4 and HF, respectively, at 200 °C. Thermal VO_2 ALE was also performed for the first time using SF_4 or HF and $Sn(acac)_2$ as the reactants. There was evidence that SF_4 is a stronger fluorination reactant than HF for VO_2 fluorination. The mass gains during the initial SF_4 and HF exposures on VO_2 ALD films were 38 and 20 ng/cm^2, respectively, at 200 °C. Thermal VO_2 ALE also had a higher etch rate when fluorinating with SF_4 compared with HF. Etch rates of 0.30 and 0.11 Å/cycle were measured for VO_2 ALE using SF_4 and HF, respectively, together with $Sn(acac)_2$ at 200 °C. Fourier transform infrared experiments were also used to monitor fluorination of the Al_2O_3 and VO_2 ALD films by SF_4 or HF. FTIR difference spectroscopy was used to observe the increase of Al−F and V−F stretching vibrations and the loss of the Al−O and V—O/V═O stretching vibrations for Al_2O_3 and VO_2, respectively, versus SF_4 or HF exposure at 200 °C. Additional absorbance features after fluorination of the Al_2O_3 ALD films by SF_4 were consistent with SF_x surface species. SF_4 is a useful fluorination agent for thermal ALE processes and can be used as an alternative to HF. In addition, SF_4 may be necessary when fluorination requires a stronger fluorination reactant than HF.

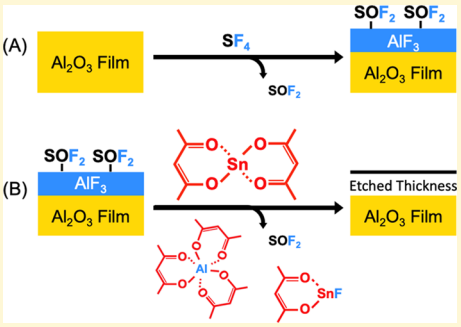

I. INTRODUCTION

Atomic layer etching (ALE) is possible using sequential and self-limiting surface reactions.[1] ALE is becoming increasingly important for advanced semiconductor manufacturing.[2] ALE can be viewed as the reverse of atomic layer deposition (ALD).[3,4] ALE can be accomplished using either plasma or thermal methods.[1,5] The first reaction during ALE usually involves surface modification by the adsorption of a reactive species that activates the surface. The second reaction during ALE is a reaction that produces a volatile etch product. In plasma ALE, the second reaction is the removal of the activated layer by sputtering using an energetic ion or neutral species.[1] Plasma ALE leads to anisotropic etching.[1] In thermal ALE, the second reaction is a reaction between a gaseous reactant and the surface layer that produces stable and volatile etching products.[5] Thermal ALE leads to isotropic etching.[6]

During thermal ALE, the main reaction that activates the surface has been fluorination. For example, thermal Al_2O_3 ALE was initially demonstrated using HF and $Sn(acac)_2$ as the reactants.[5,7] The mechanism for thermal Al_2O_3 ALE is based on fluorination and ligand-exchange reactions.[5,7] HF and $Sn(acac)_2$ have also been employed as the reactants for HfO_2 and AlN ALE.[8,9] Other metal precursors such as $Al(CH_3)_3$, $AlCl(CH_3)_2$, $SiCl_4$, and $TiCl_4$ have also been effective for the ligand-exchange reaction following fluorination with HF.[10−13] These reactants have led to Al_2O_3, HfO_2, and ZrO_2 ALE.[10−13] HF and $Al(CH_3)_3$ have also been used for SiO_2 and ZnO ALE using a "conversion-etch" mechanism, where $Al(CH_3)_3$ both is involved in ligand-exchange after fluorination and also converts the surface of the remaining substrate to Al_2O_3.[14,15]

Although HF has been useful as a fluorination reactant during thermal ALE, HF does have some drawbacks. HF is a highly corrosive gas.[16] Upon contact with moisture, HF forms hydrofluoric acid, which is also corrosive and toxic. Anhydrous HF is particularly problematic because its vapor pressure at room temperature exceeds atmospheric pressure. HF-pyridine liquid sources of HF are safer because the vapor pressure of HF above the HF-pyridine solution is 90−100 Torr at room temperature.[9] However, alternative fluorination reactants to

Received: December 22, 2018
Revised: April 11, 2019
Published: April 12, 2019

DOI: 10.1021/acs.chemmater.8b05294
Chem. Mater. 2019, 31, 3624−3635

replace HF are desirable because HF is a weak fluorination reactant.

HF is a nucleophilic fluorination reactant where the fluoride anion serves as the active reaction species. HF is a convenient fluorination reactant that can fluorinate most metal oxides or metal nitrides. HF produces metal fluorides and H_2O or NH_3 as the reaction products. However, HF is a relatively weak fluorination agent compared with other inorganic nucleophilic fluorination reactants, such as SF_4. Many electrophilic fluorinating agents also exist in which an electron-deficient fluorine serves as the active reaction species. The most widely used inorganic electrophilic fluorination reactant is F_2. Another common inorganic electrophilic fluorination reactant is XeF_2.

The standard free energy changes, $\Delta G°$, for the fluorination of a variety of materials using HF, SF_4, F_2, and XeF_2 are given in Table 1.[17] The $\Delta G°$ values are all reported at 200 °C. Most of the $\Delta G°$ values are negative except for HF fluorination of ZnS and VO_2, which have slightly positive $\Delta G°$ values. A comparison of the various $\Delta G°$ values reveals that SF_4, F_2, and XeF_2 have higher negative $\Delta G°$ values than HF for all the materials. SF_4, F_2, and XeF_2 are stronger fluorination reactants than HF and are all possible alternatives to HF.

Table 1. Fluorination Reactions for Various Metal Compounds Using HF, SF_4, F_2, and XeF_2[a]

Al_2O_3	
$Al_2O_3 + 6HF \rightarrow 2AlF_3 + 3H_2O$	$\Delta G° = -58$ kcal
$Al_2O_3 + 3SF_4 \rightarrow 2AlF_3 + 3SOF_2$	$\Delta G° = -199$ kcal
$Al_2O_3 + 3F_2 \rightarrow 2AlF_3 + 3/2O_2$	$\Delta G° = -297$ kcal
$Al_2O_3 + 3XeF_2 \rightarrow 2AlF_3 + 3Xe + 3/2O_2$	$\Delta G° = -258$ kcal
HfO_2	
$HfO_2 + 4HF \rightarrow HfF_4 + 2H_2O$	$\Delta G° = -19$ kcal
$HfO_2 + 2SF_4 \rightarrow HfF_4 + 2SOF_2$	$\Delta G° = -113$ kcal
$HfO_2 + 2F_2 \rightarrow HfF_4 + O_2$	$\Delta G° = -178$ kcal
$HfO_2 + 4XeF_2 \rightarrow HfF_4 + 4Xe + 3/2O_2$	$\Delta G° = -152$ kcal
GaN	
$GaN + 3HF \rightarrow GaF_3 + NH_3$	$\Delta G° = -40$ kcal
$GaN + 3/4SF_4 \rightarrow GaF_3 + 1/2N_2 + 3/16S_8$	$\Delta G° = -114$ kcal
$GaN + 3/2F_2 \rightarrow GaF_3 + 1/2\ N_2$	$\Delta G° = -239$ kcal
$GaN + 3/2XeF_2 \rightarrow GaF_3 + 3/2Xe + 1/2N_2$	$\Delta G° = -219$ kcal
ZnS	
$ZnS + 2HF \rightarrow ZnF_2 + H_2S$	$\Delta G° = +6$ kcal
$ZnS + 1/2SF_4 \rightarrow ZnF_2 + 3/16S_8$	$\Delta G° = -33$ kcal
$ZnS + F_2 \rightarrow ZnF_2 + 1/8S_8$	$\Delta G° = -116$ kcal
$ZnS + XeF_2 \rightarrow ZnF_2 + Xe + 1/8S_8$	$\Delta G° = -103$ kcal
VO_2	
$VO_2 + 4HF \rightarrow VF_4 + 2H_2O$	$\Delta G° = +9$ kcal
$VO_2 + 2SF_4 \rightarrow VF_4 + 2SOF_2$	$\Delta G° = -85$ kcal
$VO_2 + 2F_2 \rightarrow VF_4 + O_2$	$\Delta G° = -150$ kcal
$VO_2 + 2XeF_2 \rightarrow VF_4 + 2Xe + O_2$	$\Delta G° = -124$ kcal

[a] $\Delta G°$ values are reported at 200 °C.[17]

In this paper, SF_4 was examined as an alternative to HF. SF_4 is an effective fluorination reactant for organic carbonyl compounds and metal oxides.[18,19] Previous work has also demonstrated that SF_4 can fluorinate γ-Al_2O_3.[20] The high SF_4 vapor pressure of ∼10 atm at 25 °C also facilitates the implementation of SF_4.[21] However, although SF_4 is considered a safer alternative to HF because SF_4 has a distinct sulfur odor, SF_4 also has issues because hydrolysis of SF_4 can produce HF via $SF_4 + H_2O \rightarrow SOF_2 + 2HF$.[22]

SF_4 was used as the fluorination reactant for the thermal ALE of Al_2O_3 and VO_2. $Sn(acac)_2$ was used as the metal precursor for the ligand-exchange reaction. Al_2O_3 ALE was studied to compare SF_4 with the previous results using HF as the fluorination reactant for thermal Al_2O_3 ALE.[5,7,10,23] VO_2 ALE was also examined using HF or SF_4 and $Sn(acac)_2$ as the reactants. SF_4 may be needed as the fluorination agent for thermal VO_2 ALE. Thermochemical calculations indicate that the predicted $\Delta G°$ for the fluorination of VO_2 to VF_4 is slightly positive for HF at 200 °C.[17] In contrast, fluorination of VO_2 to VF_4 has a large negative $\Delta G°$ using SF_4 at 200 °C.[17]

Thermal VO_2 ALE is reported for the first time in this paper. VO_2 is a semiconductor at room temperature and has a metal−insulator transition around 68 °C.[24,25] This transition is accompanied by a large change in resistivity and optical transmittance. Consequently, VO_2 is a useful material for thermochromic films,[25,26] bolometers,[27,28] and switching devices.[29,30] Thermal VO_2 ALE may be useful to produce thin VO_2 films with low thermal mass and high film stability. A low thermal mass is needed for larger thermal transients when using VO_2 as a thermal sensor. Thin films employed for their metal−insulator transition are also less susceptible to fracture from stress that can result from temperature cycling and structural changes around the metal−insulator transition.

II. EXPERIMENTAL SECTION

II.A. Growth and Etching of Al_2O_3 and VO_2 Films. The initial Al_2O_3 and VO_2 films were prepared using Al_2O_3 and VO_2 ALD. The Al_2O_3 ALD films were grown using $Al(CH_3)_3$ (trimethylaluminum (TMA)) (97%, Sigma-Aldrich) and DI H_2O as the reactants at deposition temperatures between 130 and 200 °C. TMA and H_2O are known to yield amorphous Al_2O_3 ALD films at these temperatures.[31] The VO_2 ALD films were deposited using tetrakis(ethylmethylamino) vanadium (TEMAV) (Air Liquide) and DI H_2O as the reactants at 150 °C.[32] TEMAV is a useful vanadium source for VO_2 ALD because vanadium is already in the +4 oxidation state. TEMAV and H_2O are known to yield vanadium(IV) oxide films.[33] TEMAV and H_2O also yield amorphous VO_2 ALD films at 150 °C.[32,33]

ALD films were deposited and etched in a custom-built stainless steel viscous flow reactor. This reactor is similar in design to a previous viscous flow reactor built for quartz crystal microbalance (QCM) studies of ALD.[34] However, the flow tube was replaced with a circular puck-shaped chamber to accommodate 8″ wafers. The reactants and the carrier gas flow across the samples in the chamber. The chamber had a 10″ diameter and was equipped with a fast-entry load-lock door for sample loading. The QCM was positioned at the center of this chamber.

A total N_2 flow of 160 sccm was used as both a purge and inert carrier gas during the reactions and produced a reactor pressure of 1.0 Torr. The N_2 flow was controlled on each precursor line by mass flow controllers (Alicat Scientific). The N_2 flow was uniformly distributed inside the circular puck-shaped chamber using a baffle that served to limit the gas conductance. The reactor was pumped with a dual-stage mechanical pump (Alcatel Adixen Pascal 2010 C2). The pressure was monitored using a capacitance manometer (MKS Baratron 626A) on the reactor. The temperature of the reactor chamber was maintained using heaters regulated with proportional−integral−derivative (PID) control.

The stainless steel bubbler containing the TEMAV was heated to 60−65 °C to increase the vapor pressure. An N_2 flow of ∼20 sccm over the headspace of the TEMAV source was also used to increase the precursor transport. The other growth reactants were maintained at room temperature. All lines were heated to define a temperature gradient between the reactant sources and the reactor. The temperature progressively increased to prevent condensation in the dosing lines in the reactor chamber.

DOI: 10.1021/acs.chemmater.8b05294
Chem. Mater. 2019, 31, 3624−3635

Al_2O_3 ALE and VO_2 ALE were performed using sulfur tetrafluoride (SF_4, >98.5%, SynQuest Laboratories), HF-pyridine (70 wt % HF, Sigma-Aldrich), and tin(II) acetylacetonate ($Sn(acac)_2$, 99.9% trace metals basis, Sigma-Aldrich). SF_4 and HF-pyridine were maintained at room temperature. The $Sn(acac)_2$ bubbler was heated to around 100 °C to obtain adequate vapor pressure.

II.B. QCM, XPS, SE, and FTIR Measurements. The reactor chamber was equipped with an in situ quartz crystal microbalance (QCM). The QCM was an SC-cut quartz crystal (Maxtek SC-101 gold coated, 6 MHz). The frequency of the QCM was recorded using an Inficon Q-pod quartz crystal monitor. The QCM housing was a modified Inficon Cool Drawer single sensor that used N_2 flow to provide a backside purge on the crystal.[34] The housing around the crystal was sealed using high temperature silver epoxy (Epo-Tek H21D, Epoxy Technology). The additional N_2 flow from the QCM purge exited downstream from the QCM crystal and raised the reactor pressure to 1.05 Torr when only N_2 was flowing.

The VO_2 films on Si coupons were analyzed with ex situ X-ray photoelectron spectroscopy (XPS, PHI 5600) after VO_2 ALD to verify the chemical state of the film. The films were loaded into the XPS chamber within 1 h of unloading from the deposition chamber to reduce surface oxidation effects. In addition, the Al_2O_3 ALD film thicknesses were investigated with ex situ spectroscopic ellipsometry (J. A. Woollam M-2000) both before and after etching at varying temperatures to determine the temperature dependence of Al_2O_3 ALE using SF_4 and $Sn(acac)_2$ as the reactants.

In situ infrared spectroscopy was employed to monitor VO_2 ALD and the fluorination of the Al_2O_3 and VO_2 ALD films with SF_4 and HF. A description of this reactor, equipped for in situ FTIR transmission spectroscopy, has been presented earlier.[35] To increase the surface area for higher sensitivity to the surface species, the Al_2O_3 and VO_2 ALD films were deposited on silicon nanoparticles that were 30−50 nm in diameter (>98%, US Research Nanomaterials). The Si nanoparticles were initially pressed into tungsten grids.[36,37] The tungsten grids have an area of 2 × 3 cm^2 and were 50 μm thick and contained 100 grid lines per inch.

The tungsten grids were resistively heated to 150 °C for VO_2 ALD and 200 °C for SF_4 and HF fluorination of the Al_2O_3 and VO_2 ALD films. The heating was conducted using a DC power supply (6268B, 20 V/20 A, Hewlett-Packard). The voltage output of the DC power supply was controlled by a PID temperature controller (Love Controls 16B, Dwyer Instruments). The temperature was monitored with a K-type thermocouple. This thermocouple was fixed to the tungsten grid with epoxy (Ceramabond 571, Aremco). The epoxy also electrically isolated the thermocouple from the tungsten grid. The FTIR spectra were recorded at 150 °C during VO_2 ALD and at 200 °C for Al_2O_3 and VO_2 fluorination.

III. RESULTS AND DISCUSSION

III.A. Al_2O_3 ALE Using SF_4 and $Sn(acac)_2$. Figure 1 displays the mass change versus time during 100 cycles of Al_2O_3 ALE at 200 °C using SF_4 and $Sn(acac)_2$ as the reactants. The SF_4 exposures were performed at 500 mTorr for 2.5 s. The $Sn(acac)_2$ exposures were conducted at 50 mTorr for 2.5 s. After each reactant exposure, the system was purged with a viscous flow of N_2 gas at 160 sccm for 55 s. This reaction sequence is designated as 2.5−55−2.5−55. The initial Al_2O_3 film was deposited on the QCM with trimethylaluminum (TMA) and H_2O as the reactants using 150 Al_2O_3 ALD cycles. The reaction sequence for Al_2O_3 ALD was 3−55−3−55. The purge times are longer than usual because of the design and larger volume of the reactor that could accommodate 8″ silicon wafers.

The loss of mass versus time is linear in Figure 1. The slight deviations from linearity are attributed to the effect of small temperature deviations on the QCM measurements over the course of the long experiments. The average mass change per cycle (MCPC) over the 100 cycles is −6.0 ng/cm^2. This MCPC yields an etch rate of 0.20 Å/cycle. The conversion between mass and thickness used an Al_2O_3 ALD film density of 2.95 g/cm^3 determined by X-ray reflectivity (Bede D1 System). This etch rate for Al_2O_3 ALE using SF_4 and $Sn(acac)_2$ at 200 °C is very comparable with the etch rate for Al_2O_3 ALE using HF and $Sn(acac)_2$ at 200 °C. The etch rate for Al_2O_3 ALE employing HF and $Sn(acac)_2$ at 200 °C was previously measured to be 0.28 Å/cycle.[5,7]

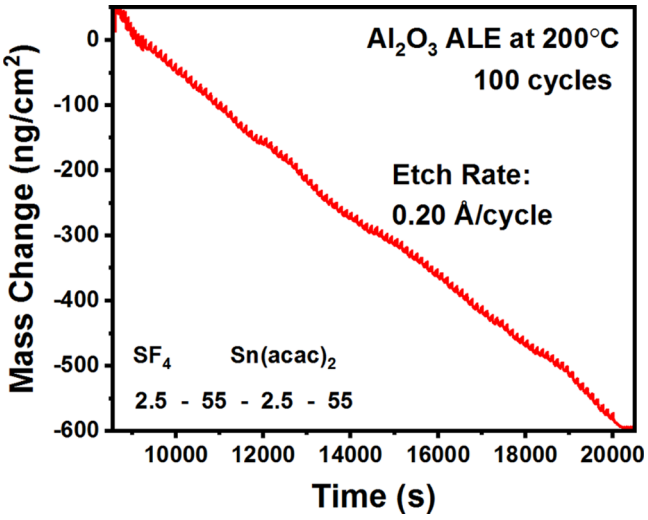

Figure 1. Mass change versus time during 100 cycles of Al_2O_3 ALE at 200 °C using SF_4 and $Sn(acac)_2$ as the reactants. Etch rate is 0.20 Å/cycle.

An expanded view of three Al_2O_3 ALE cycles from Figure 1 is shown in Figure 2. The SF_4 exposure fluorinates the Al_2O_3 surface and may produce AlF_3 or AlF_xO_y surface species. AlF_3 is a stable fluoride with a melting temperature of 1290 °C and an extremely low vapor pressure at 200 °C.[38] In addition, SF_4 should remove oxygen from Al_2O_3 through SOF_2 desorption. SOF_2 is the main reaction product from the reaction of SF_4 with metal oxides, H_2O, or oxygen-containing organic compounds.[18,19,22] SF_4 should also remove any possible acac

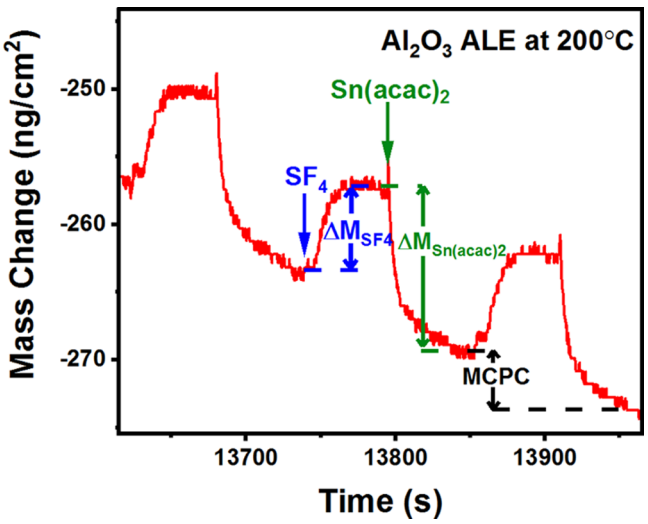

Figure 2. Expanded view of three Al_2O_3 ALE cycles from Figure 1 showing mass gain during the SF_4 exposure and mass loss during $Sn(acac)_2$ exposure.

DOI: 10.1021/acs.chemmater.8b05294
Chem. Mater. 2019, 31, 3624−3635

species on the surface from the previous $Sn(acac)_2$ exposure. The SF_4 exposure leads to a mass gain ΔM_{SF_4} = 6.2 ng/cm^2.

$Sn(acac)_2$ can then react with the fluorinated Al_2O_3 surface through ligand-exchange to form volatile SnF(acac) and $Al(acac)_3$ or $AlF(acac)_2$ species. $Al(acac)_3$ has a vapor pressure of 3.3 Torr at 150 °C and ~7 Torr at 200 °C.[39,40] The net result of the $Sn(acac)_2$ exposure is a mass loss $\Delta M_{Sn(acac)_2}$ = −12.2 ng/cm^2. The gradual mass reduction during the purge time of 55 s may be attributed to the slow desorption of acac species from the surface. Acac species were observed on Al_2O_3 surfaces during Al_2O_3 ALE using HF and $Sn(acac)_2$.[7] There was also an inverse correlation between the coverage of acac surface species and the Al_2O_3 etch rate in these previous studies that was consistent with more desorption of acac species at higher substrate temperatures.[7]

Assuming that the volatile etch products are $Al(acac)_3$, SnF(acac), and SOF_2, the overall reaction can be described as:

$$Al_2O_3 + 3SF_4 + 6Sn(acac)_2 \rightarrow 2Al(acac)_3 + 6SnF(acac) + 3SOF_2 \quad (1)$$

This overall reaction can be divided into the proposed SF_4 and $Sn(acac)_2$ reactions occurring during Al_2O_3 ALE at steady state:

$$(A)Al_2O_3{}^* + 3SF_4(g) \rightarrow 2AlF_3|xSOF_2{}^* + (3 - x)SOF_2(g) \quad (2)$$

$$(B)2AlF_3|xSOF_2{}^* + 6Sn(acac)_2(g) \rightarrow 2Al(acac)_3(g) + 6SnF(acac)(g) + xSOF_2(g) \quad (3)$$

These reactions include the surface species that change during the SF_4 and $Sn(acac)_2$ exposures. The asterisks indicate the surface species. The vertical lines separate the various surface species. To satisfy the overall reaction stoichiometry in eq 1, the ΔM_{SF_4} and $\Delta M_{Sn(acac)_2}$ values require the presence of a surface intermediate that adds mass during reaction A and subtracts mass during reaction B. SOF_2* is the most likely surface intermediate produced during the SF_4 exposure in reaction A. A schematic illustrating the proposed SF_4 and $Sn(acac)_2$ reactions is shown in Figure 3.

Al_2O_3* in eq 2 represents the amount of Al_2O_3 that is etched during the ALE reactions.[7] x quantifies the amount of SOF_2* surface species after the SF_4 exposures relative to the amount of Al_2O_3 that is etched in one Al_2O_3 ALE cycle. The parameter x can be determined by the $\Delta M_{Sn(acac)_2}$ and MCPC values using the equation:

$$x = [M_{Al_2O_3}(\Delta M_{Sn(acac)_2}/\mathrm{MCPC}) - 2M_{AlF_3}]/M_{SOF_2} \quad (4)$$

$$x = [102.0(-12.2/-6.0) - 2(84.0)]/86.1 \quad (5)$$

The values 84.0, 102.0, and 86.1 are the molecular weights in atomic mass units for AlF_3, Al_2O_3, and SOF_2, respectively. Using $\Delta M_{Sn(acac)_2}$ = −12.2 ng/cm^2 and MCPC = −6.0 ng/cm^2, eq 5 yields x = 0.46. This x value indicates that there are 0.46 SOF_2* species present on the surface after the SF_4 exposures for every Al_2O_3 unit etched during one Al_2O_3 ALE cycle.

The MCPC and etch rate during Al_2O_3 ALE at 200 °C using SF_4 and $Sn(acac)_2$ are −6.0 ng/cm^2 and 0.20 Å/cycle, respectively. This removal rate of Al_2O_3 is equivalent to 3.54 × 10^{13} Al_2O_3 units/cm^2. This removal rate is only ~5% of the number of Al_2O_3 units on the Al_2O_3 surface. An estimate for the number of Al_2O_3 units on the Al_2O_3 surface is obtained from the mass density of 3.0 g/cm^3 for Al_2O_3 ALD films. This mass density is equivalent to a number density ρ = 1.77 × 10^{22} Al_2O_3 units/cm^3. $\rho^{2/3}$ then provides an estimate for the number of Al_2O_3 units on the Al_2O_3 surface of 6.8 × 10^{14} Al_2O_3 units/cm^2. Based on the x value of 0.46, the SOF_2* coverage is determined to be 1.63 × 10^{13} SOF_2* species/cm^2. This SOF_2* coverage is only about 2.4% of the number of Al_2O_3 units on the Al_2O_3 surface.

Figure 4 demonstrates the self-limiting nature of the SF_4 and $Sn(acac)_2$ reactions during Al_2O_3 ALE. Each point represents the average mass change per cycle (MCPC) versus exposure time over 20 reaction cycles. In Figure 4a, the $Sn(acac)_2$ exposure time was held constant at 2.5 s, and the SF_4 exposure time was varied from 0 to 3 s. The purge time after each reactant exposure was 55 s. This reactant pulse sequence is designated as X−55−2.5−55. Similarly, in Figure 4b, the SF_4 exposure time was held constant at 2.5 s, and the $Sn(acac)_2$ exposure time was varied between 0 and 2.5 s. This reactant pulse sequence is denoted as 2.5−55−X−55. The MCPC levels off versus exposure time for both SF_4 and $Sn(acac)_2$. In addition, neither reactant is capable of spontaneously etching the Al_2O_3 film.

Other experiments have recently explored the effect of both exposure and pressure on Al_2O_3 fluorination using HF as the fluorination reactant.[41] These investigations have revealed that Al_2O_3 fluorination is self-limiting as a function of exposure. The fluoride thickness, y, changes according to $dy/dt = k/y$ where k is a constant that is dependent on HF pressure, $k = k_0P$. Integration of this rate equation yields the parabolic expressions $y^2(t) = 2kt$ or $y(t) = (2k_0Pt)^{1/2}$. The fluorination kinetics are restricted by the fluoride layer on the Al_2O_3 surface that acts as a diffusion barrier for further fluorination. The kinetics of Al_2O_3 fluorination are similar to the kinetics of Si oxidation that have been described by the Deal−Grove model.[42,43] Similar behavior is expected for Al_2O_3 fluorination using SF_4 as the fluorination reactant.

Figure 5 shows the first three cycles of Al_2O_3 ALE using SF_4 and $Sn(acac)_2$. The mass gain observed during the first SF_4 exposure represents the fluorination of an initial Al_2O_3 ALD film prior to any $Sn(acac)_2$ exposures. The first SF_4 exposure leads to a mass gain ΔM_{SF_4} = 35.1 ng/cm^2. The SF_4 exposure is believed to fluorinate the Al_2O_3 film according to the reaction

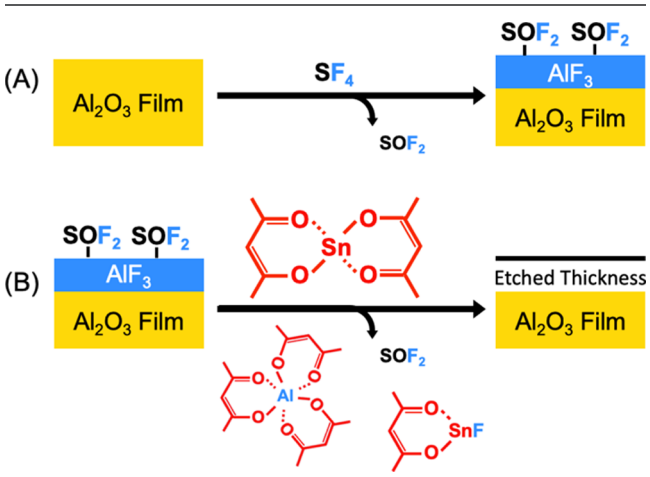

Figure 3. (A, B) Schematic of the sequential surface reactions during Al_2O_3 ALE using exposures of SF_4 and $Sn(acac)_2$.

DOI: 10.1021/acs.chemmater.8b05294
Chem. Mater. 2019, 31, 3624−3635

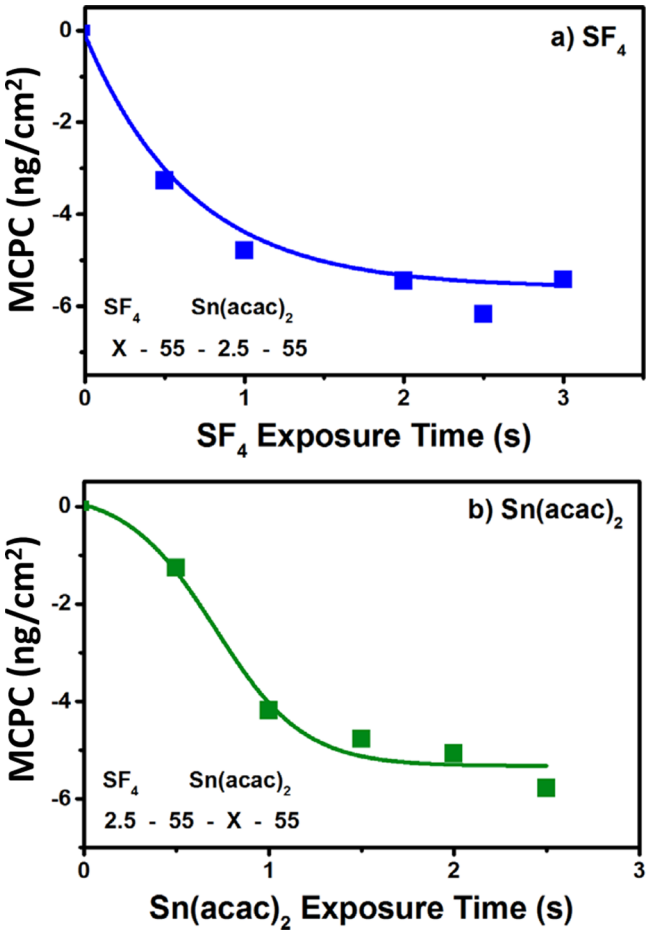

Figure 4. Mass change per cycle (MCPC) showing the self-limiting nature of the SF_4 and $Sn(acac)_2$ reactions during Al_2O_3 ALE at 200 °C. (a) SF_4 exposure time, *X*, is varied as the $Sn(acac)_2$ exposure time is held constant at 2.5 s. (b) $Sn(acac)_2$ exposure time, *X*, is varied as the SF_4 exposure time is held constant at 2.5 s. Purge times after each reactant exposure are 55 s.

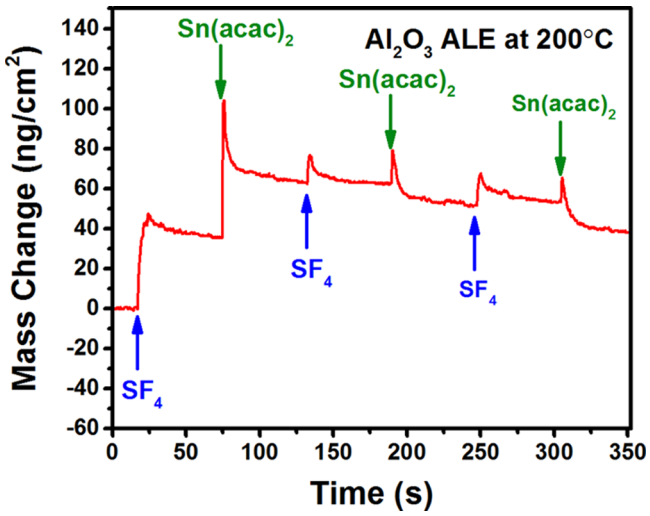

Figure 5. First three cycles of Al_2O_3 ALE using SF_4 and $Sn(acac)_2$ at 200 °C showing initial fluorination mass gain during SF_4 exposure, subsequent mass changes during the first $Sn(acac)_2$ exposure, and subsequent SF_4 and $Sn(acac)_2$ exposures.

given in Table 1: $Al_2O_3 + 3SF_4 \rightarrow 2AlF_3 + 3SOF_2$. The mass gain can be used to calculate the Al_2O_3 thickness converted to an AlF_3 thickness by the SF_4 exposure. The mass change ΔM_{SF_4} = 35.1 ng/cm^2 is consistent with the conversion of ~1.8 Å of Al_2O_3 to ~3.1 Å of AlF_3. These thicknesses are based on the change in mass of 66 g/mol during Al_2O_3 conversion to $2AlF_3$, an Al_2O_3 ALD film density of 2.95 g/cm^3 from XRR, and an AlF_3 density of 2.88 g/cm^3.

Figure 5 also shows that there is a mass gain $\Delta M_{Sn(acac)_2}$ = 27.5 ng/cm^2 for the first $Sn(acac)_2$ exposure after the initial SF_4 exposure. Although $Sn(acac)_2$ can undergo ligand exchange with the fluorinated surface, the net mass gain indicates that acac species are added to the surface during the first $Sn(acac)_2$ exposure. Subsequently, the SF_4 and $Sn(acac)_2$ exposures for the second and third reaction cycles are evolving to the steady-state etching behavior observed in Figure 2. This nucleation period occurs over approximately six reaction cycles.

Fluorination of the Al_2O_3 ALD film with SF_4 and HF was also monitored with in situ FTIR spectroscopy. Figure 6a

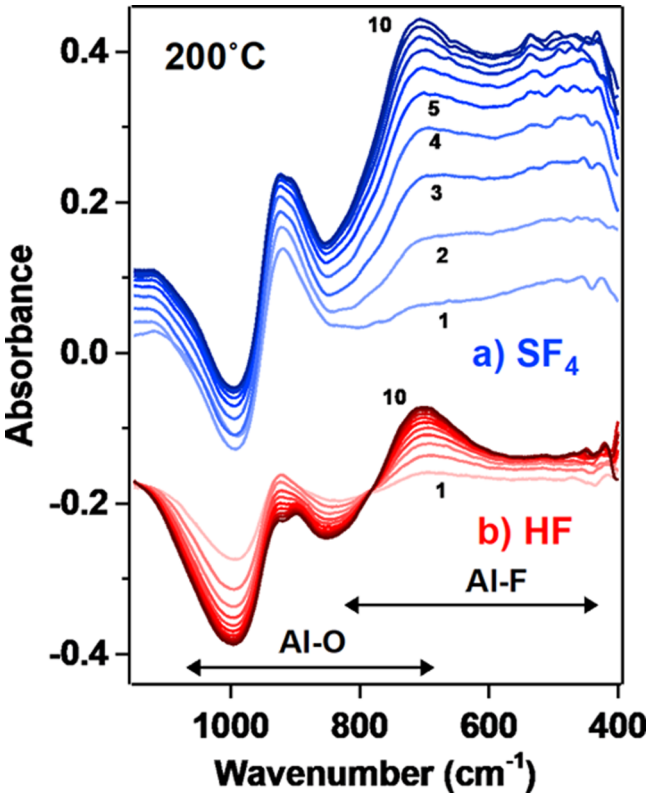

Figure 6. FTIR spectra recorded at 200 °C during fluorination of the Al_2O_3 ALD film at 200 °C. (a) Difference spectra for 10 SF_4 exposures on the Al_2O_3 ALD film. (b) Difference spectra for 10 HF exposures on the Al_2O_3 ALD film.

shows the difference spectra for 10 SF_4 exposures on the Al_2O_3 ALD film at 200 °C. Each SF_4 exposure was performed at 300 mTorr for 1 s. The difference spectra were obtained by subtracting the spectra after each SF_4 exposure from the spectrum for the initial Al_2O_3 ALD film. These difference spectra show the progressive fluorination of the Al_2O_3 ALD film by the SF_4 exposures according to the proposed reaction $Al_2O_3 + 3SF_4 \rightarrow 2AlF_3 + 3SOF_2$.

DOI: 10.1021/acs.chemmater.8b05294
Chem. Mater. 2019, 31, 3624−3635

Figure 6a demonstrates that a broad absorbance peak becomes larger at ~700 cm^{-1} with increasing SF_4 exposures. This absorbance peak is assigned to an Al−F stretching vibration.[44,45] An additional absorbance peak is observed at ~900 cm^{-1}. A broad shoulder is also present at frequencies between 400 and 600 cm^{-1} that are less than the frequency of the Al−F stretching vibration. These absorbance features are attributed to the presence of SF_x species on the AlF_3 surface. SF_2 stretching vibrations are observed in SF_4 at ~890 and ~860 cm^{-1}.[46,47] Additional stretching and deformation vibrational modes exist for SF_4 at ~560 and ~530 cm^{-1}.[46,47] Likewise, a strong symmetric FSO deformation mode has been reported in SOF_2 at ~530 cm^{-1}.[48,49]

Figure 6a also shows that a prominent absorbance loss occurs at ~1000 cm^{-1}. This absorbance loss is attributed to the reduction of absorbance from Al−O stretching vibrations in Al_2O_3.[13] In addition, there is an increase in the background absorbance during SF_4 fluorination. This baseline shift is larger than the progressive loss of Al−O stretching vibrations with increasing SF_4 exposures in Figure 6a. The origin of this increasing background absorbance with increasing SF_4 exposures is not understood at this time.

For comparison, Figure 6b shows difference spectra for 10 HF exposures on the Al_2O_3 ALD films at 200 °C. These difference spectra have been displayed for clarity in presentation. Each HF exposure was conducted at 100 mTorr for 1 s. The difference spectra were obtained by subtracting the spectra after each HF exposure from the spectrum recorded for the initial Al_2O_3 ALD film. These difference spectra are consistent with the progressive fluorination of the Al_2O_3 ALD film by HF exposures according to the reaction $Al_2O_3 + 6HF \rightarrow 2AlF_3 + 3H_2O$. The HF exposures may also fluorinate the Al_2O_3 ALD film to produce oxyfluorides by the reaction $Al_2O_3 + zHF \rightarrow 2AlO_{(6-z)/4}F_{z/2} + (z/2)H_2O$.[50]

The absorbance peak from the Al−F stretching vibration in Figure 6b is located at ~700 cm^{-1}.[13,44,45] This absorbance peak progressively becomes larger with increasing HF exposures. A prominent absorbance loss also occurs at ~1000 cm^{-1} resulting from the progressive loss of Al−O stretching vibrations from Al_2O_3 with increasing HF exposure.[13] In contrast to the results for SF_4, absorbance gains at ~900 cm^{-1} and between 400 and 600 cm^{-1} are not observed for HF fluorination of Al_2O_3 because there are no SF_x surface species. There is also no increase in the background absorbance during HF fluorination.

Figure 7 shows results for the temperature dependence of Al_2O_3 ALE using SF_4 and $Sn(acac)_2$. These results were obtained using spectroscopic ellipsometry (SE) measurements with Al_2O_3 ALD films on Si wafers. A spectroscopic ellipsometer was used to measure film thicknesses both before and after etching. The samples were initially coated with Al_2O_3 ALD films at 130 °C. The individual samples were then etched for various numbers of cycles at temperatures from 150 to 225 °C prior to the SE measurements. The Al_2O_3 etch rates increased with temperature. The etch rates were 0.04 Å/cycle at 150 °C, 0.07 Å/cycle at 175 °C, 0.14 Å/cycle at 200 °C, and 0.25 Å/cycle at 225 °C. The etch rate of 0.14 Å/cycle at 200 °C from these SE measurements is less than the etch rate of 0.2 Å/cycle from the QCM analysis in Figure 1. The SE measurements in Figure 7 provide the trends versus temperature but are not as accurate as the QCM analysis because they are based on only 2−3 data points.

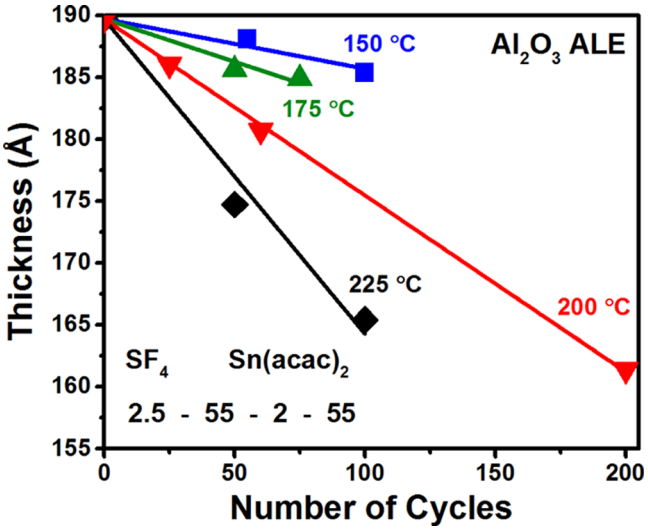

Figure 7. Temperature dependence of Al_2O_3 ALE using SF_4 and $Sn(acac)_2$. Etch rate increases from 0.04 Å/cycle at 150 °C to 0.25 Å/cycle at 225 °C.

An Arrhenius plot of these temperature-dependent etch rates yields an activation barrier of 44 kcal/mol. This activation barrier of 44 kcal/mol could result from the temperature dependence of the fluorination reaction. Higher temperatures should produce progressively thicker fluoride layers on Al_2O_3. If these fluoride layers are removed during the ligand-exchange reaction, then the Al_2O_3 etch rates would be expected to be temperature-dependent. The activation barrier may also be associated with the $Sn(acac)_2$ ligand-exchange reaction. The ligand-exchange reaction may leave acac species on the Al_2O_3 surface that may block the etching.[7] Removing these acac species would then increase the etching. The thermal desorption of these acac species may produce temperature-dependent Al_2O_3 etch rates.[7]

III.B. VO_2 ALD Using TEMAV and H_2O. VO_2 ALD films were grown using TEMAV and H_2O prior to the VO_2 ALE studies. Figure 8 shows the linear growth of VO_2 ALD films at

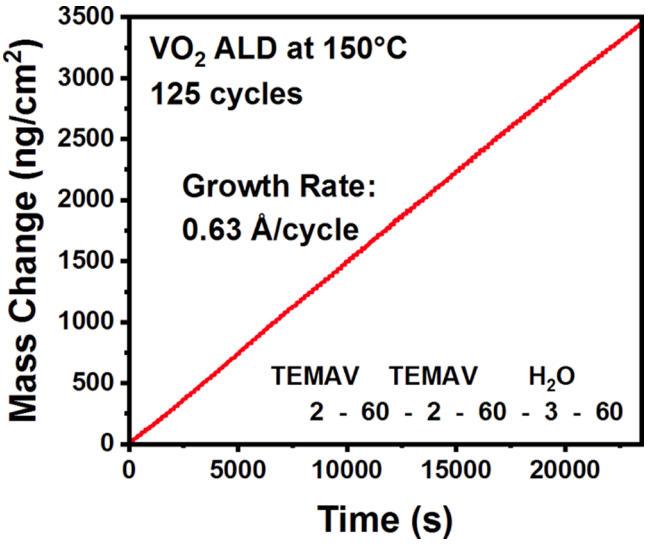

Figure 8. Mass change versus time during 125 cycles of VO_2 ALD at 150 °C using TEMAV and H_2O as the reactants. Growth rate is 0.63 Å/cycle.

DOI: 10.1021/acs.chemmater.8b05294
Chem. Mater. 2019, 31, 3624−3635

150 °C for 125 reaction cycles. Each reaction cycle consisted of two 2 s TEMAV exposures, followed by a 60 s N_2 gas purge, a 3 s H_2O exposure, and then a 60 s purge. The TEMAV pressure was 25 mTorr. Two exposures of TEMAV were used for every reaction cycle to ensure that the surface reaction reached completion. The H_2O pressure was 100 mTorr. The mass gain per cycle is 27.4 ng/cm^2. This mass gain per cycle is consistent with a VO_2 growth rate of 0.63 Å/cycle. This growth rate is based on a film density of 4.36 g/cm^3 measured by XRR. This growth rate is in agreement with the previously reported VO_2 ALD growth rate of 0.67 Å/cycle using TEMAV and H_2O at 150 °C.[32,33]

X-ray photoelectron spectroscopy (XPS) was used to confirm the stoichiometry of the VO_2 films. Figure 9 shows the XPS spectrum in the O 1s and V 2p regions. Curve fittings of the O 1s and V 2p regions are consistent with mostly a VO_2 film with a small component of V_2O_5. The percentages were 94.4% VO_2 and 5.6% V_2O_5. The peak position was calibrated using the O 1s binding energy set at 530 eV with a single Shirley background over the entire O 1s and V 2p areas. The vanadium(IV) oxide and vanadium(V) oxide V $2p_{1/2}$−V $2p_{3/2}$ splitting was fixed at 7.33 eV and the $2p_{1/2}$ to $2p_{3/2}$ ratio was fixed at 2:1.[51,52]

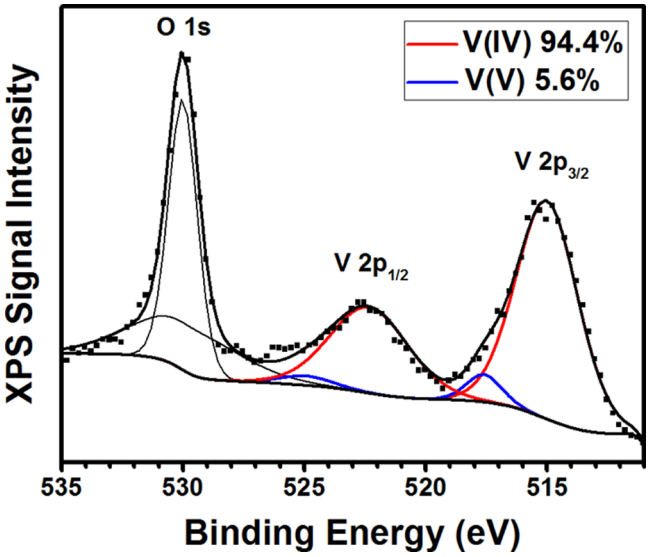

Figure 9. XPS spectrum of VO_2 ALD film in the O 1s and V 2p regions. Quantification of the V $2p_{3/2}$ peak indicates 94.4% VO_2 (V^{4+}) and 5.6% V_2O_5 (V^{5+}).

The growth of the VO_2 ALD films using TEMAV and H_2O at 150 °C was also investigated using in situ FTIR spectroscopy. The TEMAV exposure was performed at 10 mTorr for 2 s. The H_2O exposure was defined with a pressure of 100 mTorr for 1 s. A 60 s viscous flow N_2 purge at 1 Torr was employed after each reactant exposure. The FTIR spectra were also recorded after each reactant exposure.

Figure 10 shows the FTIR spectra at 150 °C after every 5 cycles of VO_2 ALD using TEMAV and H_2O for a total of 35 cycles. The spectra shown in Figure 10 were obtained after the H_2O exposures. There is a strong and broad absorbance that is centered at approximately 630 cm^{-1}. This absorbance peak progressively increases with the number of ALD cycles. This absorbance feature is attributed to V−O stretching vibrations.[53,54] Earlier infrared vibrational spectroscopy studies of crystalline VO_2 demonstrated that the vibrational spectrum of VO_2 becomes featureless in the metallic state above the metal−insulator transition at 68 °C.[54] In contrast, vibrational features are observed in Figure 10 for the amorphous VO_2 films at 150 °C. However, evidence of an increase in the background absorbance was observed from 400 to 4000 cm^{-1} during VO_2 ALD.

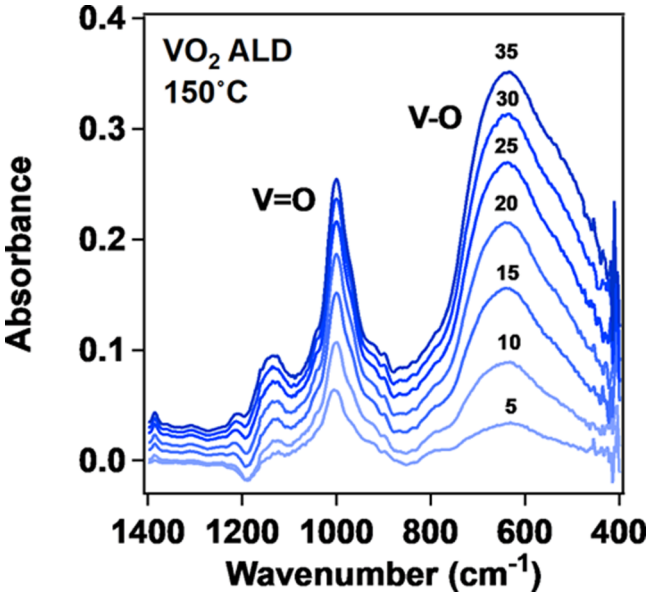

Figure 10. FTIR spectra recorded at 150 °C after every 5 cycles of VO_2 ALD for 35 cycles using TEMAV and H_2O as the reactants at 150 °C.

Absorbance from another vibrational mode centered at ∼996 cm^{-1} also increases mostly during the initial cycles of VO_2 ALD. This absorbance feature is attributed to V═O vibrations.[53,55] The V═O vibration is associated with a terminal oxygen that is likely at the surface of the VO_2 ALD film.[53,55] During the later cycles of VO_2 ALD, this absorbance is increasing more slowly because of some V═O vibrations in the VO_2 film and because of the increasing background absorbance. The frequency of the V═O vibration is also associated with the oxidation state of the vanadium.[53] The observation of the V═O vibrational feature at ∼996 cm^{-1} may be an indicator for vanadium in the +4 oxidation state.[53]

III.C. VO_2 ALE Using SF_4 or HF and Sn(acac)$_2$. Etching of the VO_2 ALD films was performed using SF_4 or HF and Sn(acac)$_2$ as the reactants. Figure 11 shows the mass change versus time during VO_2 ALE using SF_4 and Sn(acac)$_2$ as the reactants at 200 °C. The reactant exposure sequence was 3−55−3−55. The SF_4 pressure was 500 mTorr. The Sn(acac)$_2$ pressure was ∼50 mTorr. Figure 11 reveals that a linear mass loss is observed during VO_2 ALE over 50 cycles. The average MCPC is −13.2 ng/cm^2 for the 50 cycles. Based on a VO_2 ALD film density of 4.36 g/cm^3 from XRR measurements, the etch rate is 0.30 Å/cycle at 200 °C. Additional experiments revealed that the etch rates were in the self-limiting regime for SF_4 and Sn(acac)$_2$ exposures of 3 s.

An expanded view of three VO_2 ALE cycles from Figure 11 is shown in Figure 12. The SF_4 exposure leads to a mass gain ΔM_{SF_4} = 9.8 ng/cm^2. This mass gain is attributed to fluorination of the VO_2 surface to VF_4 or a VO_xF_y oxyfluoride. VF_4 is a fairly stable metal fluoride with a melting temperature at 325 °C. SF_4 may also leave SOF_2 on the surface similar to

DOI: 10.1021/acs.chemmater.8b05294
Chem. Mater. 2019, 31, 3624−3635

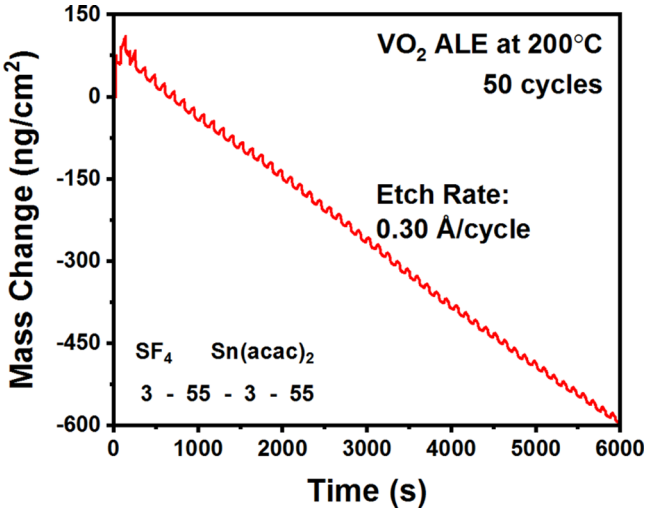

Figure 11. Mass change versus time during VO_2 ALE using SF_4 and $Sn(acac)_2$ as the reactants at 200 °C. Etch rate is 0.30 Å/cycle.

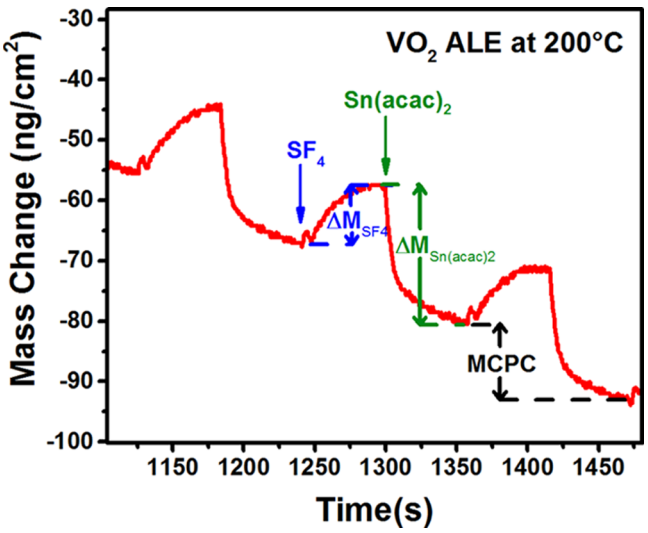

Figure 12. Expanded view of three VO_2 ALE cycles from Figure 11 showing mass gain during the SF_4 exposure and mass loss during $Sn(acac)_2$ exposure.

the proposed reactions for Al_2O_3 ALE using SF_4 and $Sn(acac)_2$. The subsequent $Sn(acac)_2$ exposure then produces a mass loss $\Delta M_{Sn(acac)_2} = -23.1$ ng/cm^2. This mass loss is consistent with $Sn(acac)_2$ removing the VF_4 surface layer by a ligand-exchange reaction along with any SOF_2 surface species to produce volatile products such as $VF_2(acac)_2$, SnF(acac), and SOF_2. There is very little information on $VF_2(acac)_2$ in the literature. However, $VCl_2(acac)_2$ is used in the synthesis of other vanadium compounds.[56,57] The $Sn(acac)_2$ exposure may also lead to SnF(acac) species adsorbed on the VO_2 surface.

If the volatile etch products are $VF_2(acac)_2$, SnF(acac), and SOF_2, the overall reaction can be written as

$$VO_2 + 2SF_4 + 2Sn(acac)_2 \rightarrow VF_2(acac)_2 + 2SnF(acac) + 2SOF_2 \quad (6)$$

This overall reaction can then be divided into the proposed SF_4 and $Sn(acac)_2$ reactions occurring during VO_2 ALE at steady state

$$(A)VO_2{}^* + 2SF_4 \rightarrow VF_4|xSOF_2{}^* + (2 - x)SOF_2 \quad (7)$$

$$(B)VF_4|xSOF_2{}^* + 2Sn(acac)_2 \rightarrow VF_2(acac)_2 + 2SnF(acac) + xSOF_2 \quad (8)$$

These reactions include the surface species that are believed to change during the SF_4 and $Sn(acac)_2$ exposures. The asterisks again indicate the surface species, and the vertical lines separate the various surface species. Assuming the reaction stoichiometry given in eq 6, the ΔM_{SF_4} and $\Delta M_{Sn(acac)_2}$ values require a surface intermediate that adds mass during reaction A and subtracts mass during reaction B. Therefore, $SOF_2{}^*$ is included as a surface intermediate in eqs 7 and 8.

$VO_2{}^*$ shown in eq 7 is the amount of VO_2 that is etched during the ALE reactions.[7] x quantifies the amount of $SOF_2{}^*$ species on the surface after the SF_4 exposure relative to the amount of VO_2 that is etched in one VO_2 ALE cycle. The parameter x can be determined by the $\Delta M_{Sn(acac)_2}$ and MCPC values using the equation:

$$x = [M_{VO_2}(\Delta M_{Sn(acac)_2}/\mathrm{MCPC}) - M_{VO_2}]/M_{SOF_2} \quad (9)$$

$$x = [82.9(-23.1/-13.2) - 126.9]/86.1 \quad (10)$$

The values 126.9, 82.9, and 86.1 are the molecular weights for VF_4, VO_2, and SOF_2, respectively. Using $\Delta M_{Sn(acac)_2} = -23.1$ ng/cm^2 and MCPC = −13.2 ng/cm^2, eq 10 yields $x = 0.21$. This x value reveals that there are 0.21 $SOF_2{}^*$ species present on the surface after the SF_4 exposures for every VO_2 unit etched during one VO_2 ALE cycle.

The MCPC and etch rate during VO_2 ALE at 200 °C using SF_4 and $Sn(acac)_2$ are −13.2 ng/cm^2 and 0.30 Å/cycle, respectively. This removal rate of VO_2 is equivalent to 9.58×10^{13} VO_2 units/cm^2. The density of the VO_2 ALD films is 4.36 g/cm^3 from XRR measurements. This density yields an estimate of 1.00×10^{15} VO_2 units/cm^2 for the number of VO_2 units on the VO_2 surface. The VO_2 removal rate is about 9.6% of the number of VO_2 units on the VO_2 surface. Based on the x value of 0.21, the $SOF_2{}^*$ coverage is determined to be 2.01×10^{13} $SOF_2{}^*$ species/cm^2. This $SOF_2{}^*$ coverage is about 2.0% of the number of VO_2 units on the VO_2 surface.

The mass changes during the SF_4 and $Sn(acac)_2$ exposures decrease slightly as the etching proceeds. However, the MCPC stays nearly constant at −13.2 ng/cm^2 averaged over the 50 cycles in Figure 11. The slight decrease in the mass changes during the SF_4 and $Sn(acac)_2$ exposures may result from slow changes in the surface composition. There is a possibility that the $Sn(acac)_2$ reactant may be able to remove some vanadium species from the VO_2 film as vanadyl acetylacetonate ($VO(acac)_2$). The removal of $VO(acac)_2$ would change the V/O ratio on the surface and perhaps slowly affect the etch rate.

III.D. Fluorination of VO_2 Using SF_4 or HF. QCM experiments explored the effect of SF_4 exposure on an initial VO_2 ALD film independent of any acac surface species. Figure 13 shows the first three VO_2 ALE cycles on an initial VO_2 ALD film using SF_4 and $Sn(acac)_2$ as the reactants. The first SF_4 exposure leads to a mass gain $\Delta M_{SF_4} = 38.5$ ng/cm^2 at 200 °C. The SF_4 exposure was conducted at 500 mTorr for 3 s. The SF_4 exposure is believed to fluorinate the VO_2 film according to the reaction given in Table 1: $VO_2 + 2SF_4 \rightarrow VF_4 + 2SOF_2$. The mass gain can be used to calculate the VO_2 thickness

DOI: 10.1021/acs.chemmater.8b05294
Chem. Mater. 2019, 31, 3624−3635

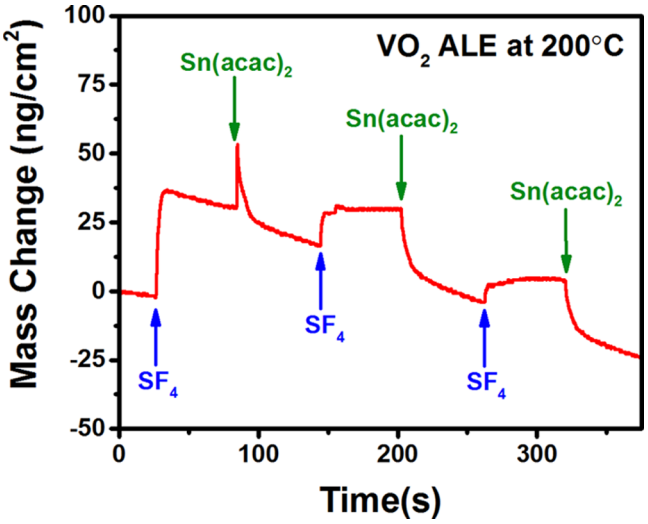

Figure 13. First three cycles of VO_2 ALE using SF_4 and $Sn(acac)_2$ at 200 °C showing initial mass gain from fluorination during SF_4 exposure and mass changes during the first $Sn(acac)_2$ exposure and subsequent SF_4 and $Sn(acac)_2$ exposures.

converted to VF_4 by the SF_4 exposure. The mass change of ΔM_{SF_4} = 38.5 ng/cm^2 is consistent with the conversion of ~1.6 Å of VO_2 to ~3.7 Å of VF_4. These thicknesses are based on the change in mass of 44 g/mol during VO_2 conversion to VF_4, a VO_2 ALD film density of 4.36 g/cm^3 from XRR, and a VF_4 density of 2.98 g/cm^3.

Figure 14 shows additional QCM measurements that compare the mass gain during the fluorination of the initial

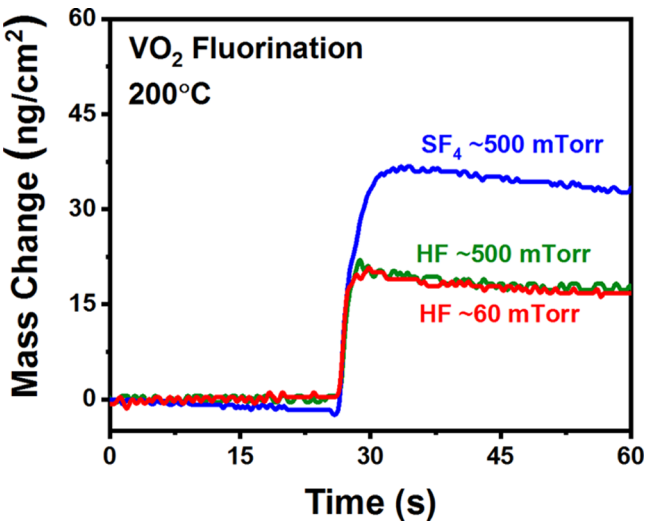

Figure 14. Mass gains during fluorination of the initial VO_2 ALD film with either SF_4 or HF. SF_4 exposure at 500 mTorr leads to a higher mass gain than HF exposures at either 60 or 500 mTorr.

VO_2 ALD film using either SF_4 or HF. The SF_4 exposure at 500 mTorr leads to a much higher mass gain than the HF exposures at either 60 or 500 mTorr. The mass gain resulting from the SF_4 exposures is 38.5 ng/cm^2. The mass gain from the HF exposures is 20.5 ng/cm^2 and is independent of the HF pressure. The higher mass gain from the SF_4 exposures probably cannot be explained solely by the presence of SOF_2* species on the VO_2 surface. The SOF_2* coverage of 2.01 × 10^{13} SOF_2* species/cm^2 present after the SF_4 exposures during steady state VO_2 ALE using SF_4 and $Sn(acac)_2$ is equivalent to a mass of 2.9 ng/cm^2.

The ability of the HF to fluorinate the VO_2 ALD film was initially questioned because the $\Delta G°$ value for the VO_2 + 4HF → VF_4 + $2H_2O$ reaction is positive at $\Delta G°$ = +9 kcal. The mass gain with HF exposure suggests that other fluorination reactions may be possible. For example, a subfluoride of vanadium may be formed from the reaction VO_2 + HF → VOF_2 + H_2O. This reaction has a negative standard free energy value $\Delta G°$ = −1.58 kcal/mol at 200 °C.

To explore further the VO_2 fluorination, in situ FTIR spectroscopy studies were used to monitor the fluorination of VO_2 ALD films with SF_4 and HF at 200 °C. Figure 15 displays

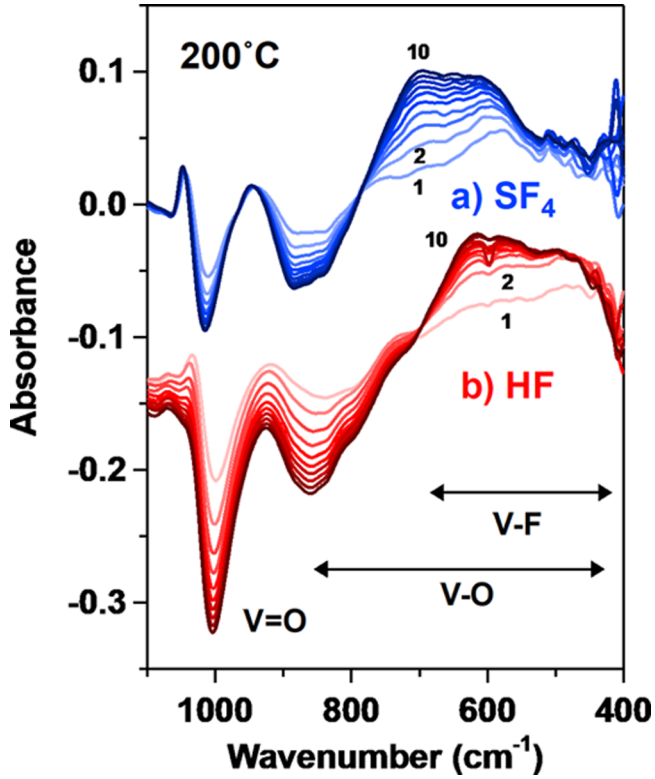

Figure 15. FTIR spectra recorded at 200 °C during fluorination of the VO_2 ALD film at 200 °C. (a) Difference spectra for 10 SF_4 exposures on the VO_2 ALD film. (b) Difference spectra for 10 HF exposures on the VO_2 ALD film.

the fluorination of the VO_2 ALD film using either SF_4 or HF exposures. Figure 15a shows the difference spectra for the fluorination using 10 consecutive SF_4 exposures. Each SF_4 exposure was defined by a pressure of 300 mTorr for 1 s. Figure 15b shows the difference spectra for the progressive fluorination using 10 consecutive HF exposures. These difference spectra have been displaced for clarity in presentation. Each HF exposure was defined by a pressure of 100 mTorr for 1 s. The reference spectrum for the difference spectra in Figures 15a and 15b was the spectrum of the initial VO_2 ALD film.

Broad absorbance gains centered at ~650 and ~590 cm^{-1} are observed for both SF_4 and HF exposures, respectively. This absorbance gain is consistent with V−F stretching vibrations. Previous investigations have observed the V−F stretching vibration at 530 cm^{-1} in VF_4 and at 540 cm^{-1} in VF_3.[58] The

DOI: 10.1021/acs.chemmater.8b05294
Chem. Mater. 2019, 31, 3624−3635

slightly higher frequencies observed during the fluorination of VO_2 ALD films may be attributed to the presence of oxyfluorides and the higher V−F frequencies in vanadium oxyfluorides.[59] In comparison with the results for SF_4 on Al_2O_3 ALD films displayed in Figure 6a, no prominent absorbance gains are observed at ∼900 cm^{-1} or 530−560 cm^{-1} in Figure 15a that would be consistent with an abundance of SF_x surface species.[46−49] The absence of these absorbance gains is consistent with the lower x value for VO_2 ALE using SF_4 and $Sn(acac)_2$.

Another prominent absorbance feature in Figure 15 is the absorbance loss at ∼1000 cm^{-1} after both SF_4 and HF exposures. The loss of this V═O stretching vibration would be expected during fluorination if the V═O vibrational modes are primarily on the surface of the VO_2 ALD film. Fluorination with SF_4 also produces a small absorbance gain in the difference spectrum in Figure 15a at ∼1045 cm^{-1}. This absorbance gain may again be indicative of vanadium oxyfluorides with vanadium atoms bonded to both oxygen and fluorine atoms.[59]

IV. CONCLUSIONS

Fluorination and ligand-exchange reactions can be employed for thermal ALE. HF has been the most common fluorination reactant. However, HF is a fairly weak nucleophilic fluorination reactant. Stronger fluorination reactants may be useful as an alternative to HF. One possible option is SF_4. The thermal ALE of Al_2O_3 and VO_2 was explored using both SF_4 and HF as fluorination reactants together with $Sn(acac)_2$ as the metal precursor for ligand-exchange.

SF_4 and HF were very comparable as fluorination reactants during Al_2O_3 ALE. The mass gains during the initial fluorination of Al_2O_3 ALD films at 200 °C were 35 and 38 ng/cm^2 using SF_4 and HF, respectively. In addition, the etch rates for Al_2O_3 ALD films using SF_4 and HF, together with $Sn(acac)_2$, were 0.20 and 0.28 Å/cycle, respectively, at 200 °C. SF_4 is an effective alternative to HF for Al_2O_3 thermal ALE.

SF_4 was also compared to HF for VO_2 ALE. The mass gains during the initial SF_4 and HF exposures on VO_2 ALD films were 38 and 20 ng/cm^2, respectively. The larger fluorination when using SF_4 also led to higher VO_2 etch rates. Etch rates of 0.30 and 0.11 Å/cycle were measured for VO_2 ALE using SF_4 and HF, respectively, together with $Sn(acac)_2$ at 200 °C. The more favorable thermochemistry for VO_2 fluorination by SF_4 leads to a larger etch rate.

Additional FTIR experiments were also conducted to observe the fluorination of the Al_2O_3 and VO_2 ALD films by SF_4 or HF. These studies revealed that SF_4 and HF were comparable as fluorination reactants. The FTIR difference spectra were used to monitor the growth of Al−F and V−F stretching vibrations and the loss of Al−O and V═O stretching vibrations for Al_2O_3 and VO_2, respectively, versus SF_4 or HF exposure. The FTIR difference spectra also suggested that S−F stretching vibrations from SF_x surface species were present on Al_2O_3 after SF_4 exposures. SF_4 is a useful fluorination reactant for thermal ALE. SF_4 is also a stronger fluorination reactant that may be needed for etching some materials.

■ AUTHOR INFORMATION

Corresponding Author

*E-mail: steven.george@colorado.edu.

ORCID

Jonas C. Gertsch: 0000-0002-0626-9655

Steven M. George: 0000-0003-0253-9184

Notes

The authors declare no competing financial interest.

■ ACKNOWLEDGMENTS

This research was funded by the U.S. Army Research Laboratory and the U.S. Army Research Office under Contract Number W911NF-14-C-0007. Additional support was provided by the National Science Foundation through Grant CHE-1609554.

■ REFERENCES

(1) Kanarik, K. J.; Lill, T.; Hudson, E. A.; Sriraman, S.; Tan, S.; Marks, J.; Vahedi, V.; Gottscho, R. A. Overview of Atomic Layer Etching in the Semiconductor Industry. *J. Vac. Sci. Technol., A* **2015**, *33*, No. 020802.

(2) Carver, C. T.; Plombon, J. J.; Romero, P. E.; Suri, S.; Tronic, T. A.; Turkot, R. B., Jr. Atomic Layer Etching: An Industry Perspective. *ECS J. Solid State Sci. Technol.* **2015**, *4*, N5005−N5009.

(3) Faraz, T.; Roozeboom, F.; Knoops, H. C. M.; Kessels, W. M. M. Atomic Layer Etching: What Can We Learn from Atomic Layer Deposition? *ECS J. Solid State Sci. Technol.* **2015**, *4*, N5023−N5032.

(4) George, S. M. Atomic Layer Deposition: An Overview. *Chem. Rev.* **2010**, *110*, 111−131.

(5) Lee, Y.; George, S. M. Atomic Layer Etching of Al_2O_3 Using Sequential, Self-Limiting Thermal Reactions with $Sn(acac)_2$ and Hydrogen Fluoride. *ACS Nano* **2015**, *9*, 2061−2070.

(6) Zywotko, D. R.; Faguet, J.; George, S. M. Rapid Atomic Layer Etching of Al_2O_3 Using Sequential Exposures of Hydrogen Fluoride and Trimethylaluminum with No Purging. *J. Vac. Sci. Technol., A* **2018**, *36*, No. 061508.

(7) Lee, Y.; DuMont, J. W.; George, S. M. Mechanism of Thermal Al_2O_3 Atomic Layer Etching Using Sequential Reactions with $Sn(acac)_2$ and HF. *Chem. Mater.* **2015**, *27*, 3648−3657.

(8) Johnson, N. R.; Sun, H.; Sharma, K.; George, S. M. Thermal Atomic Layer Etching of Crystalline Aluminum Nitride Using Sequential, Self-limiting Hydrogen Fluoride and $Sn(acac)_2$ Reactions and Enhancement by H_2 and Ar Plasmas. *J. Vac. Sci. Technol., A* **2016**, *34*, No. 050603.

(9) Lee, Y.; DuMont, J. W.; George, S. M. Atomic Layer Etching of HfO_2 Using Sequential, Self-Limiting Thermal Reactions with $Sn(acac)_2$ and HF. *ECS J. Solid State Sci. Technol.* **2015**, *4*, N5013−N5022.

(10) Lee, Y.; DuMont, J. W.; George, S. M. Trimethylaluminum as the Metal Precursor for the Atomic Layer Etching of Al_2O_3 Using Sequential, Self-Limiting Thermal Reactions. *Chem. Mater.* **2016**, *28*, 2994−3003.

(11) Lee, Y.; George, S. M. Thermal Atomic Layer Etching of HfO_2 Using HF for Fluorination and $TiCl_4$ for Ligand-Exchange. *J. Vac. Sci. Technol., A* **2018**, *36*, No. 061504.

(12) Lee, Y.; Huffman, C.; George, S. M. Selectivity in Thermal Atomic Layer Etching Using Sequential, Self-Limiting Fluorination and Ligand-Exchange Reactions. *Chem. Mater.* **2016**, *28*, 7657−7665.

(13) DuMont, J. W.; George, S. M. Competition Between Al_2O_3 Atomic Layer Etching and AlF_3 Atomic Layer Deposition Using Sequential Exposures of Trimethylaluminum and Hydrogen Fluoride. *J. Chem. Phys.* **2017**, *146*, No. 052819.

(14) DuMont, J. W.; Marquardt, A. E.; Cano, A. M.; George, S. M. Thermal Atomic Layer Etching of $SiO_2$by a "Conversion-Etch" Mechanism Using Sequential Reactions of Trimethylaluminum and Hydrogen Fluoride. *ACS Appl. Mater. Interfaces* **2017**, *9*, 10296−10307.

(15) Zywotko, D. R.; George, S. M. Thermal Atomic Layer Etching of ZnO by a "Conversion-Etch" Mechanism Using Sequential

DOI: 10.1021/acs.chemmater.8b05294
Chem. Mater. 2019, 31, 3624−3635

Exposures of Hydrogen Fluoride and Trimethylaluminum. *Chem. Mater.* **2017**, *29*, 1183−1191.
(16) Na, J. Y.; Woo, K. H.; Yoon, S. Y.; Cho, S. Y.; Song, I. U.; Kim, J. A.; Kim, J. S. Acute Symptoms After a Community Hydrogen Fluoride Spill. *Annals of Occupational and Environmental Medicine* **2013**, *25*, 17.
(17) *HSC Chemistry*; HSC Chemistry 5.1, Outokumpu Research Oy: Pori, Finland, 2002.
(18) Hasek, W. R.; Smith, W. C.; Engelhardt, V. A. The Chemistry of Sulfur Tetrafluoride. II. The Fluorination of Organic Carbonyl Compounds[1]. *J. Am. Chem. Soc.* **1960**, *82*, 543−551.
(19) Oppegard, A. L.; Smith, W. C.; Muetterties, E. L.; Engelhardt, V. A. The Chemistry of Sulfur Tetrafluoride.[1] IV. Fluorination of Inorganic Oxides and Sulfides. *J. Am. Chem. Soc.* **1960**, *82*, 3835−3838.
(20) Bendada, A.; Webb, G.; Winfield, J. M. Fluorination of Gamma-Alumina by Sulphur Tetrafluoride, Thionyl Fluoride, Carbonyl Fluoride or Anhydrous Hydrogen Fluoride: A Radiotracer Study. *Eur. J. Solid State Inorg. Chem.* **1996**, *33*, 907−916.
(21) Tullock, C. W.; Fawcett, F. S.; Smith, W. C.; Coffman, D. D. The Chemistry of Sulfur Tetrafluoride. I. The Synthesis of Sulfur Tetrafluoride. *J. Am. Chem. Soc.* **1960**, *82*, 539−542.
(22) Roberts, H. L. The Chemistry of Compounds Containing Sulphur-Fluorine Bonds. *Q. Rev., Chem. Soc.* **1961**, *15*, 30−55.
(23) George, S. M.; Lee, Y. Prospects for Thermal Atomic Layer Etching Using Sequential, Self-Limiting Fluorination and Ligand-Exchange Reactions. *ACS Nano* **2016**, *10*, 4889−4894.
(24) Morin, F. J. Oxides Which Show a Metal-to-Insulator Transition at the Neel Temperature. *Phys. Rev. Lett.* **1959**, *3*, 34−36.
(25) Soltani, M.; Chaker, M.; Haddad, E.; Kruzelesky, R. V. Thermochromic Vanadium Dioxide Smart Coatings Grown on Kapton Substrates by Reactive Pulsed Laser Deposition. *J. Vac. Sci. Technol., A* **2006**, *24*, 612−617.
(26) Manning, T. D.; Parkin, I. P.; Pemble, M. E.; Sheel, D.; Vernardou, D. Intelligent Window Coatings: Atmospheric Pressure Chemical Vapor Deposition of Tungsten-Doped Vanadium Dioxide. *Chem. Mater.* **2004**, *16*, 744−749.
(27) Chen, C.; Yi, X.; Zhao, X.; Xiong, B. Characterizations of VO_2-Based Uncooled Microbolometer Linear Array. *Sens. Actuators, A* **2001**, *90*, 212−214.
(28) Kats, M. A.; Sharma, D.; Lin, J.; Genevet, P.; Blanchard, R.; Yang, Z.; Qazilbash, M. M.; Basov, D. N.; Ramanathan, S.; Capasso, F. Ultra-Thin Perfect Absorber Employing a Tunable Phase Change Material. *Appl. Phys. Lett.* **2012**, *101*, 221101.
(29) Jerominek, H.; Picard, F.; Vincent, D. Vanadium Oxide Films for Optical Switching and Detection. *Opt. Eng.* **1993**, *32*, 2092−2100.
(30) Yang, Z.; Ko, C. Y.; Ramanathan, S. Oxide Electronics Utilizing Ultrafast Metal-Insulator Transitions, In *Annual Review of Materials Research*, Clarke, D. R., Fratzl, P., Eds. Harvard University, 2011; *41* p. 337−367.
(31) Miikkulainen, V.; Leskelä, M.; Ritala, M.; Puurunen, R. L. Crystallinity of Inorganic Films Grown by Atomic Layer Deposition: Overview and General Trends. *J. Appl. Phys.* **2013**, *113*, No. 021301.
(32) Blanquart, T.; Niinistö, J.; Gavagnin, M.; Longo, V.; Heikkilä, M.; Puukilainen, E.; Pallem, V. R.; Dussarrat, C.; Ritala, M.; Leskelä, M. Atomic Layer Deposition and Characterization of Vanadium Oxide Thin Films. *RSC Adv.* **2013**, *3*, 1179−1185.
(33) Rampelberg, G.; Deduytsche, D.; De Schutter, B.; Premkumar, P. A.; Toeller, M.; Schaekers, M.; Martens, K.; Radu, I.; Detavernier, C. Crystallization and Semiconductor-Metal Switching Behavior of Thin VO_2 Layers Grown by Atomic Layer Deposition. *Thin Solid Films* **2014**, *550*, 59−64.
(34) Elam, J. W.; Groner, M. D.; George, S. M. Viscous Flow Reactor with Quartz Crystal Microbalance for Thin Film Growth by Atomic Layer Deposition. *Rev. Sci. Instrum.* **2002**, *73*, 2981−2987.
(35) DuMont, J. W.; George, S. M. Pyrolysis of Alucone Molecular Layer Deposition Films Studied Using In Situ Transmission Fourier Transform Infrared Spectroscopy. *J. Phys. Chem. C* **2015**, *119*, 14603−14612.
(36) Ballinger, T. H.; Wong, J. C. S.; Yates, J. T. Transmission infrared spectroscopy of High Area solid surfaces. A Useful Method for Sample Preparation. *Langmuir* **1992**, *8*, 1676−1678.
(37) Ferguson, J. D.; Weimer, A. W.; George, S. M. Atomic Layer Deposition of Ultrathin and Conformal Al_2O_3 Films on BN Particles. *Thin Solid Films* **2000**, *371*, 95−104.
(38) Brunetti, B.; Piacente, V.; Scardala, P. Torsion Vapor Pressures and Sublimation Enthalpies of Aluminum Trifluoride and Aluminum Trichloride. *J. Chem. Eng. Data* **2009**, *54*, 940−944.
(39) Berg, E. W.; Truemper, J. T. Vapor Pressure-Temperature Data for Various Metal β-diketone Chelates. *Anal. Chim. Acta* **1965**, *32*, 245−252.
(40) Fahlman, B. D.; Barron, A. R. Substituent Effects on the Volatility of Metal β-diketonates. *Adv. Mater. Opt. Electr.* **2000**, *10*, 223−232.
(41) Cano, A. M.; Marquardt, A. E.; DuMont, J. W.; George, S. M. Effect of HF Pressure on Thermal Al_2O_3 Atomic Layer Etch Rates and Al_2O_3 Fluorination. *J. Phys. Chem. C* **2019**, *123*, 10346−10355.
(42) Deal, B. E.; Grove, A. S. General Relationship for the Thermal Oxidation of Silicon. *J. Appl. Phys.* **1965**, *36*, 3770−3778.
(43) Massoud, H. Z.; Plummer, J. D.; Irene, E. A. Thermal Oxidation of Silicon in Dry Oxygen Growth-Rate Enhancement in the Thin Regime. *J. Electrochem. Soc.* **1985**, *132*, 2685−2693.
(44) Gross, U.; Rüdiger, S.; Kemnitz, E.; Brzezinka, K. W.; Mukhopadhyay, S.; Bailey, C.; Wander, A.; Harrison, N. Vibrational Analysis Study of Aluminum Trifluoride Phases. *J. Phys. Chem. A* **2007**, *111*, 5813−5819.
(45) Heitmann, W. Vacuum Evaporated Films of Aluminum Fluoride. *Thin Solid Films* **1970**, *5*, 61−67.
(46) Berney, C. V. SF_4 - Vibrational Spectra and Structure of the Solid. *J. Mol. Struct.* **1972**, *12*, 87−97.
(47) Christe, K. O.; Willner, H.; Sawodny, W. Sulfur Tetrafluoride. Assignment of Vibrational Spectra and Force Field. *Spectrochim. Acta, Part A* **1979**, *35*, 1347−1351.
(48) O'Hara, T. J., III; Noftle, R. E. The Vibrational Spectrum of thionynyl Fluoride and Its Oxygen-18 isotopomer[1]. *J. Fluorine Chem.* **1982**, *20*, 149−156.
(49) Pace, E. L.; Samuelson, H. V. Fundamental Frequency Assignment of Thionyl Fluoride (SOF_2). *J. Chem. Phys.* **1966**, *44*, 3682−3685.
(50) Kondati Natarajan, S.; Elliott, S. D. Modeling the Chemical Mechanism of the Thermal Atomic Layer Etch of Aluminum Oxide: A Density Functional Theory Study of Reactions during HF Exposure. *Chem. Mater.* **2018**, *30*, 5912−5922.
(51) Biesinger, M. C.; Lau, L. W. M.; Gerson, A. R.; Smart, R. S. C. Resolving Surface Chemical States in XPS Analysis of First Row Transition Metals, Oxides and Hydroxides: Sc, Ti, V, Cu and Zn. *Appl. Surf. Sci.* **2010**, *257*, 887−898.
(52) Silversmit, G.; Depla, D.; Poelman, H.; Marin, G. B.; De Gryse, R. Determination of the V2p XPS Binding Energies for Different Vanadium Oxidation States (V^{5+} to V^{0+}). *J. Electron Spectrosc. Relat. Phenom.* **2004**, *135*, 167−175.
(53) Botto, I. L.; Vassallo, M. B.; Baran, E. J.; Minelli, G. IR Spectra of VO_2 and V_2O_3. *Mater. Chem. Phys.* **1997**, *50*, 267−270.
(54) Hewston, T. A.; Nadler, M. P. Variable-Temperature Infrared Spectra of VO_2. *J. Solid State Chem.* **1987**, *71*, 278−281.
(55) Beattie, I. R.; Gilson, T. R. Oxide Phonon Spectra. *J. Chem. Soc. A* **1969**, 2322−2327.
(56) Hambley, T. W.; Hawkins, C. J.; Kabanos, T. A. Synthetic, Structural, and Physical Studies of Tris(2,4-pentanedionato)-vanadium(IV) Hexachloroantimonate(V) and Tris(1-phenyl-1,3-butanedionato)vanadium(IV) Hexachloroantimonate(V). *Inorg. Chem.* **1987**, *26*, 3740−3745.
(57) Sharma, N.; Sood, A. K.; Bhatt, S. S.; Kalia, S. B.; Chaudhry, S. C. Bis(2,4-pentanedionato)vanadium(IV) Aryloxides. *Transition Met Chem.* **1998**, *23*, 557−560.
(58) Cavell, R. G.; Clark, H. C. Infrared Spectra of Vanadium Fluorides. *Inorg. Chem.* **1964**, *3*, 1789−1791.

DOI: 10.1021/acs.chemmater.8b05294
Chem. Mater. 2019, 31, 3624−3635

(59) Selig, H.; Claassen, H. H. Infrared Spectra of VOF_3 and POF_3. *J. Chem. Phys.* **1966**, *44*, 1404−1406.

DOI: 10.1021/acs.chemmater.8b05294
Chem. Mater. 2019, 31, 3624−3635